Catalysis Today 419 (2023) 114153

Contents lists available at ScienceDirect

Catalysis Today

journal homepage: www.elsevier.com/locate/cattod

Layered-double hydroxides and derived oxide as CRM-free highly active catalysts for the reduction of 4-nitrophenol

Elisabetta Orfei [a,b], Andrea Fasolini [a,b,*], Salvatore Abate [c], Nikolaos Dimitratos [a,b], Francesco Basile [a,b,*]

[a] Dipartimento di Chimica Industriale "Toso Montanari", Alma Mater Studiorum - Università di Bologna, Viale Risorgimento 4, 40136 Bologna, Italy
[b] Center for Chemical Catalysis - C3, Alma Mater Studiorum - Università di Bologna, Viale del Risorgmento 4, 40136 Bologna, Italy
[c] Department of ChiBioFarAM (Industrial Chemistry), University of Messina, ERIC aisbl and INSTM/CASPE, Viale F. Stagno d'Alcontres 31, 98166 Messina, Italy

ARTICLE INFO

Keywords:
Layered-double hydroxides
4-Nitrophenol reduction
Coprecipitation
NiCuAl mixed oxide
Wastewater treatment
Cu-Ni interaction

ABSTRACT

The present study investigates the possibility to abate 4-nitrophenol (4NP), a well-known persistent contaminant in wastewaters, using Layered-Double Hydroxides (LDH) based catalysts, non-noble metals-based and Critical Raw Materials-free materials used for 4NP reduction with $NaBH_4$. It is reported the study of the effects of several parameters on the overall reaction kinetic by in situ monitoring of the 4NP reduction through UV-Vis Spectroscopy, as: (i) LDH's trivalent and divalent cation nature, (ii) LDH thermal treatment, (iii) substrate/catalyst ratio, and (iv) stirring rate. The reasons that led to increased activity were identified and correlated with catalyst's structure characterization. The results pointed out that LDH enhance synergic effect of nickel and copper by increasing reducibility which is further raised when defective mixed oxide by calcination is obtained. This resulted in enhanced 4NP reduction which could be further increased by calcination providing a highly reducible mixed oxide.

1. Introduction

In the last few decades, more and more people are becoming concerned about water pollution by organic compounds related to industrial activities, particularly in developing countries [1–3]. An example of these alarming xenobiotic compounds is represented by 4-nitrophenol (4NP), an organic pollutant already listed as an environmentally important toxic compound. 4NP is currently exceeding the concentration limits established by the law in several industrial effluents, and, despite its well-known danger, it is still largely employed for the manufacturing of drugs, dyes, leathers, insecticides (such as ethyl and methyl parathion), and even explosives [4,5].

This pollutant is a slightly yellow substance quite stable and soluble in water, characteristics associated to its easy infiltration in both surface and groundwater, as well as its unlikely biodegradation [4,6,7].

Currently, the traditional wastewater treatment strategies seem to be not effective enough for this recalcitrant compound. Thus, innovative approaches such as the catalytic reduction of the nitro group into an ammine, have attracted increasing attention. The resulting 4-aminophenol (4AP), besides being a much less worrying compound, could also been recovered and employed for the production of paracetamol, dyes, pigments, and agrochemicals, representing thereby a remarkable example of closed-loop process [8,9].

The 4NP reduction in aqueous solution is also considered a *model reaction* for catalytic efficiency tests since it shows the following interesting benefits [8,10]: (i) it does not work without a catalyst due to its intrinsic high energy activation barrier related to the repulsive forces between the 4-nitrophenolate anion and the hydride, used as reducing agent; (ii) it is a single step reaction; (iii) it does not show any co- and by-products; (iv) it follows a pseudo 1st order kinetic when one of the reagents ($NaBH_4$) can be used in large excess and, consequently, its concentration can be assumed constant during time. Thus, albeit this reaction should theoretically be of the 2nd order, due to the just explained feature, it fits a 1st order kinetic trend when sodium borohydride is used as the chosen reducing agent; (v) both 4-nitrophenolate and 4-aminophenolate are chromophores, hence, an in-situ reaction

Abbreviations: 4AP, 4-aminophenol; 2NP, 2-nitrophenol; 3NP, 3-nitrophenol; 4NP, 4-nitrophenol; LDH, Layered-Double Hydroxides.

* Corresponding authors at: Dipartimento di Chimica Industriale "Toso Montanari", Alma Mater Studiorum - Università di Bologna, Viale Risorgimento 4, 40136 Bologna, Italy

E-mail addresses: andrea.fasolini2@unibo.it (A. Fasolini), f.basile@unibo.it (F. Basile).

https://doi.org/10.1016/j.cattod.2023.114153
Received 25 November 2022; Received in revised form 29 March 2023; Accepted 6 April 2023
Available online 11 April 2023

monitoring is possible through UV-Vis analysis. Indeed, 4NP shows an intense absorption peak at 400 nm, whereas the product shows an absorption peak at 300 nm; (vi) it is a relatively fast reaction (5–60 min) and it could be directly performed in a UV–vis quartz cuvette; (vii) the reaction can be carried out in water and at room temperature.

The 4NP reduction to 4AP mechanism is still under study, but the kinetic and mechanistic studies carried out by Wunder et al. on metal nanoparticles have highlighted a Langmuir-Hinshelwood mechanism for the reaction [10,11]. The mechanism highlights that sodium borohydride is responsible for both 4NP deprotonation and hydrogen production on the surface of the catalyst [12,13]. Then, once 4NP reaches the catalyst surface too, it reacts with atomic hydrogen giving, after desorption from the catalyst surface, 4AP.

At the moment the most employed class of catalysts for the 4NP reduction into 4-aminophenol is represented by metallic nanoparticles, which increases the catalyst cost and use platinum group metals [14–24]. In this paper, we have considered non-noble, and CRM-free metal based Layered-Double Hydroxides (LDHs) worthy candidates for this reaction. Indeed, LDHs have been used in this field only as supports for the actual active phase, until now [25,26], while no one has still exploited these materials directly for them catalytic activity. It goes without saying that LDHs could present several benefits if compared to their current competitors, namely a lower production cost, a quite extended and optimised structure tunability, no need of a support to increase resistance and stability, a higher filterability from the reaction mixture, and, hence, a potentially higher reusability. Here, we report for the first time, the catalytic performance of highly active Ni-based layered-double hydroxides and of the respective oxide obtained through calcination of the LDH.

Layered-Double Hydroxides (Fig. 1) are a class of anionic clays consisting in positively charged metal hydroxide layers (M^{2+} octahedra sharing edges with a partial M^{3+}/M^{2+} substitution) and interlayer anions (A^{2-}) for charge compensation, the latter, together with water molecules, are considered to randomly move, with oxygen atoms mainly located in between two hydroxyl groups of the adjacent layer [27]. LDHs are described by the following general formula: $[M(II)_{1-x}M(III)_x(OH)_2]^{x+}(A^{n-}_{x/n})\cdot mH_2O$. LDHs are known for their tuneable composition and properties and, hence, their wide range of applications, namely anion exchangers [28], molecular sieves, catalyst supports[29], flame retardants [27], electrochemical sensors [30], drug delivery [31], polymers filling [32], and, more recently, catalysis [33–41] and photocatalysis [42–51]. In catalysis, LDHs and their thermal decomposition products (i.e. mixed oxides) are applied for basic catalysis (polymerization of alkene oxides [52], aldol condensation [53]), reforming of hydrocarbons [33,54,55], hydrogenation reactions (production of methane, methanol, higher alcohols, paraffins and olefines from syngas, hydrogenation of nitrobenzene) [56–58], oxidation reactions[59–61], exhausted gas treatment [62], support for Ziegler-Natta catalysts [27, 63].

The LDHs employed in this work have been prepared following a facile and industrially scalable co-precipitation technique, tuning both the chemical nature and ratio of the metallic cations constituting the layers of the structure. Catalytic activity of the catalysts was studied through the reduction of 4NP to 4AP using $NaBH_4$ as the reducing agent and systemic analysis of the catalyst's composition and reaction parameters have been carried out to enhance the catalytic performances. Characterizations of the catalysts have been performed to confirm the obtainment of the desired LDH or oxide phase, as well as to explain the differences in catalytic performance observed during the reaction tests. In particular, a synergetic effect given by the presence of Ni and Cu together has been shown to increase the catalytic activity in the 4NP reduction reaction.

2. Material and methods

2.1. Materials

Na_2CO_3 (CAS number: 497–19–8, Sigma Aldrich) has been used as

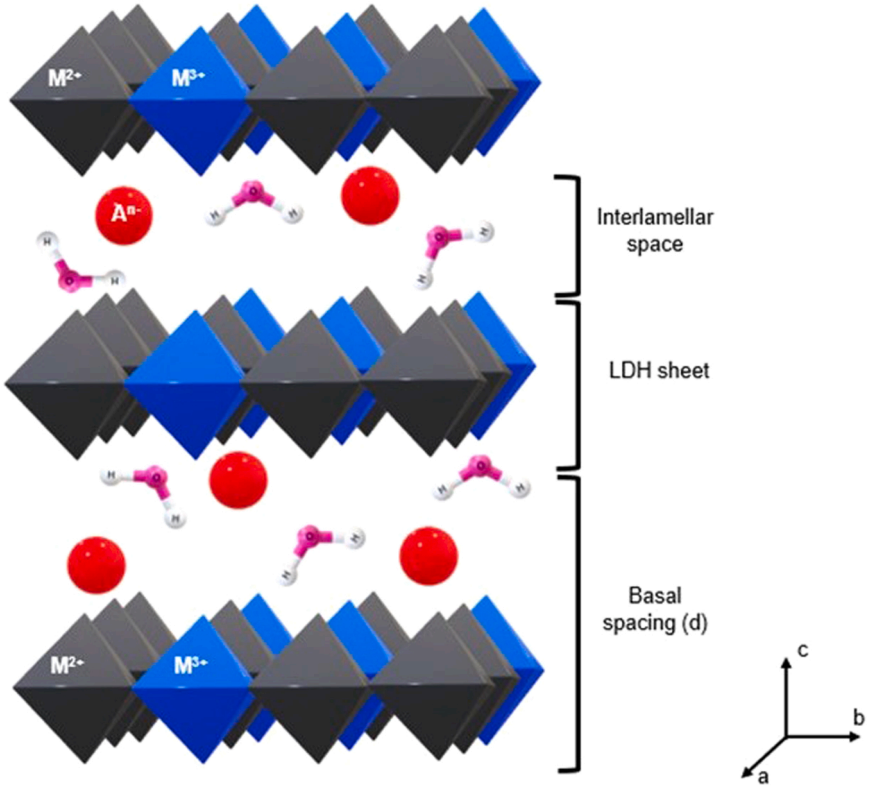

Fig. 1. Layered Double Hydroxide structure.

precursors for intercalated anions; while nickel(II) nitrate hexahydrate (Sigma Aldrich), copper(II) nitrate pentahydrate (Sigma Aldrich), zinc (II) nitrate hexahydrate (Sigma Aldrich), iron(II) nitrate nonahydrate (Sigma Aldrich), aluminium(III) nitrate nonahydrate (Sigma Aldrich), and gallium(III) nitrate (Sigma Aldrich) have been used as divalent and trivalent metallic cations. During the catalytic tests the following materials were used: sodium borohydride ($NaBH_4$, 99%, Sigma Aldrich), 2-nitrophenol (>99%, Sigma Aldrich), 3-nitrophenol (>99%, Sigma Aldrich), 4-nitrophenol (>99%, Sigma Aldrich).

2.2. Catalysts preparation

LDHs have been prepared following a co-precipitation method. A 1 M solution of Na_2CO_3 is placed on a heating plate fixed at 56 °C. The pH is then adjusted until the desired convenient value is reached with nitric acid. The pH value of 9.5 is decided according to the Kps of the metallic (Ni, Cu, Ga, Al, etc.) hydroxides to make them precipitate. Then, the solution containing the metallic nitrates, in the right proportion, is dropped from a dropping funnel in the first beaker. During the dropping, the pH is maintained fixed by continuously adding NaOH 3 M with a pipette. When the addition is over, the solution is stirred for 1 h at 56 °C ("*aging*"). Afterwards, the solid is filtered over a Buckner funnel and washed with distilled water. The solid is dried over the Buckner and eventually put in an oven at 75 °C overnight.

The LDH calcination has been performed at 400 °C for 3 h, heating through a thermal ramp of 2 °C/min under static air conditions.

2.3. Catalysts characterization

Powder X-ray diffraction analysis (XRPD) was performed using the Philips PW1050/81 diffractometer equipped with a graphite monochromator and controlled by the PW1710 detection unit (Cu Kα, $\lambda = 0.15418$ nm). A range of 2θ from 5° to 80° was investigated at a scanning rate of 0.05°/s. The XRPD analyses on the spent catalysts have been performed using a Buker D2 Phaser diffractometer equipped with a Lynx-eye 1D detector. A range of 2θ from 5° to 80° was investigated at a scanning rate of 2°/s.

The surface area of the catalysts has been calculated through a nitrogen physisorption analysis. The analysis has been carried out through a SORPTY 1750 (Fisons Instruments) on samples with a mass of about 0.1 g.

The redox properties of the catalysts used during 4-nitrophenol reduction tests were studied carrying out temperature programmed reduction/oxidation (TPRO) cycles. The analyses were carried out using a ThermoQuest Instrument TPD/R/O 1100 Catalytic Surface Analyzer. Before running any reduction/oxidation step, any sample was subjected to a pre-treatment, flowing He (30 mL/min) while the temperature was increased from room temperature to 150 °C and kept at this temperature for half a hour. Afterwards, the sample was cooled down to 60 °C. Then, TPR/O/R cycles were performed introducing into the system a 5% H_2/Ar (30 mL/min), while the operating temperature was increased from 60 °C to 950 °C at the rate of 10 °C/min. An isotherm at this final temperature of 30 min was performed. After, the system was purged with He, while the temperature reached 60 °C. TPR was followed by temperature programmed oxidation (TPO). A 5% O_2/He (30 mL/min) was introduced into the system, and, like the TPR, the temperature was increased from 60 °C to 950 °C at the rate of 10 °C/min. After 30 min of isotherm, the sample was cooled down until 60 °C in He, in order to perform the final step of reduction.

PHI VersaProbe II (Physical Electronics), equipped with an Al Kα (1486.6 eV) X-ray source, measured the XPS spectra. The survey spectra were recorded with an analyser energy path of 117 eV, while the C1s, O1s, Cu2p and Ni2p, core levels were measured at 23.5 eV passing energy. The X-ray beam size was 100 μm at 25 W. A charge neutralization procedure was performed by simultaneous irradiation of samples using a low-energy electron beam and an ion beam before measuring the spectra. The position of the XPS peaks was referenced to graphitic Carbon (284.80 eV). XPS peaks were deconvoluted by using the Multipack Data Reduction Software (ULVAC-PHI, Inc), employing a Shirley background curve.

TEM analyses were carried out using a TEM/STEM FEI TECNAI F20 microscope combined with Energy Dispersive X – Ray Spectrometry (EDS), at 200 keV. The sample preparation was carried out by suspending the powder in ethanol and treating it with ultrasound for 15 min and then depositing it on a metallic grid.

The leaching of the reaction solution was analysed using an Inductively coupled plasma mass spectrometry (ICP-MS)7900 instrument from Agilent Technologies in He mode. The instrument has been calibrated using Ni standard solutions, commercially available from Agilent technologies.

2.4. Catalytic tests

2.4.1. Calibration

UV–visible spectroscopic analyses were performed in a 1 cm path length cuvette using an in-situ Agilent Cary 3500 UV-Vis Spectrometer. The extinction coefficient was determined by a calibration performed with sample at known concentrations from which we got a value of 18,100 M^{-1} cm^{-1} which is close to the literature value of 18,000 M^{-1} cm^{-1} [64].

2.4.2. Kinetic studies

The 4NP stock solution has been prepared solubilizing 0.1391 g of 4-nitrophenol in 100 mL of distilled water in a volumetric flask. Then, 0.5 mL of the previously prepared solution have been diluted in a 25-mL matrass with distilled water. In a second 25-mL volumetric flask, 0.0085 g of $NaBH_4$ have been solubilised in distilled water to obtain a solution of $9.0 \cdot 10^{-3}$ M [65]. These two solutions have been mixed in a beaker in which also 0.010 g of catalyst have been added. The final solution has been mixed with a pipette. Afterwards, a part of this solution has been collected and added in a UV–VIS quartz cuvette to monitor the kinetics of 4-nitrophenol reduction. A reference solution for the UV-Vis measurements has been prepared with a $9.0 \cdot 10^{-3}$ M $NaBH_4$ water solution. A spectrum is automatically recorded every minute at 25 °C until a satisfactory conversion is reached. Recycling tests have been carried out by recovering the used catalyst at the end of reaction, from both the cuvette and the beaker used to homogenize the reagents. The catalyst has been separated by filtration over a Buckner funnel and, after calcination of the recovered powder at 400 °C for 1 h, the catalyst has been placed in a fresh solution of 4NP and $NaBH_4$. The just described procedure has been repeated at the end of every recycling test. The first reaction, and consequently also the following ones, has been performed using 1 mg of catalyst. The catalytic activity was compared with the apparent kinetic constant and the conversion reached after a reaction time of 240 s

3. Results and discussion

3.1. Catalysts characterization

The coprecipitation technique was used to prepare the layered double hydroxide catalysts, namely NiAl 3:1, NiGa 3:1, NiCuAl 1.5:1.5:1, NiCuAl 2.25:0.75:1, ZnCuAl 1.5:1.5:1, and NiFe 3:1 (atomic ratio) with intercalated carbonate anions, and XRD analyses have been carried out to confirm the obtainment of LDH structure in our materials. In general, among the possible metallic cations suitable for LDH preparation, we have selected Ni and Cu as divalent cations and Al, Fe or Ga as trivalent cations due to the following reasons: (i) they are inexpensive and reliable materials, with a view of a possible future technology scale-up, i.e., they are not Critical Raw Materials (CRMs) or Platinum Group Metals (PGMs), and, moreover, (ii) their use as active materials' supports for the 4NP reduction reaction is already reported in the literature

[26,66,67].

Fig. 2 **a** shows the XRD patterns obtained from X-ray diffraction analyses of the coprecipitated samples, which, indeed, confirmed the formation of the LDH structure showing the characteristic diffraction peaks of this phase. In fact, the XRD patterns present the typical diffraction peaks of NiAl LDH according to JCPDS file [15–87], which is characterized by diffraction peaks at 11.5° (003), 23.0° (006), 35.1° (012), 39.7° (015), 47.4° (018), 61.4° (110), 62.1° (113), 65.9° (1016), and 72.3° (202), with small shifts toward higher 2θ given by the presence of different cations, namely Cu^{2+} and Zn^{2+}, that show a smaller radius with respect to Ni^{2+}, or Fe^{3+} and Ga^{3+}, exhibit a bigger radius with respect to Al^{3+}. Nevertheless, all the characteristic reflections of the crystalline phase are still distinguishable, confirming also in the cases of NiCuAl, ZnCuAl, NiFe, or NiGa LDHs the formation of the desired LDH structure. In particular, three intense diffraction peaks at low values of 2θ are peculiar features of LDHs. The first of these, with Miller indices 003, provides information about the basal d spacing. Furthermore, d_{003} spacing values calculated for each sample agree with those found in the literature, namely around 0.75 nm for intercalated carbonate anions. Fe-based LDHs' XRD patterns show an intense background noise that is due to the fluorescence effect caused by the interaction of copper X-ray source with iron.

The corresponding mixed oxide was obtained from NiCuAl 1.5:1.5:1 LDH by calcination at 400 °C. The oxide's XRD pattern (Fig. 2**b**) presents the typical diffraction peaks of nickel oxide according to JCPDS file [15–87] which is characterized by diffraction peaks at 37.2° (111), 43.8° (200), and 63.2° (220). Cu and Al partially substitute Ni in its cubic cell. Indeed, according to the Bragg law, the lower the distance between two adjacent crystallographic planes, i.e., the lower the cation size as in the case of copper and aluminium compared to nickel, the lower is the d space among the plane families and the higher is the X-ray incidence ray (θ). Therefore, a small shift in the NiCuAl mixed oxide XRD pattern towards higher 2θ values was noticed if compared to the nickel oxide one listed before. Average crystal size was calculated by the Debye-Scherrer formula and was found to be proportional to the copper amount with dimensions of 5.3 nm, 5.0 nm, and 4.2 nm respectively for NiAl 3:1, NiCuAl 2.25:0.75:1, and NiCuAl 1.5:1.5:1. This is consistent with what was already reported in the literature[68]. In addition, the formation of an oxide further reduced the crystallite size from 4.2 nm to 3.5 nm for the NiCuAl 1.5:1.5:1 sample due to the formation of a 3D structure and the collapse of the 2D LDH's layers.

Nitrogen physisorption analyses have been carried out for the prepared samples to investigate the morphological properties and the surface area values are reported in Table 1. They show that the presence of aluminium as trivalent cation (M^{3+}) in the LDH structure enhances the LDH's surface area. In general, different surface areas are obtained when the composition of the LDH is changed. Nevertheless, the highest surface area is obtained for the NiCuAl 1.5:1.5:1 mixed oxide. Calcination is in fact responsible for the high mixed oxide's surface area, related to the porosity created during the release of carbon dioxide by decomposition of the carbonate ions in what is called a cratering effect, which occurs in correspondence of the collapse of the hydroxide layers to form the corresponding oxide [27].

Table 1
BET-Surface area values of the prepared samples.

Sample	Surface area (m^2/g)
Ni Al 3:1 LDH	123
Ni Ga 3:1 LDH	78
Ni Fe 3:1 LDH	44
Ni Cu Al 1.5:1.5:1 LDH	76
Ni Cu Al 2.25:0.75:1 LDH	103
Zn Cu Al 1.5:1.5:1 LDH	60
Ni Cu Al 1.5:1.5:1 oxide	120

The reducibility of the synthesized catalysts was analysed by temperature-programmed reduction (TPR).

Comparing the reducibility of the different LDHs (Fig. 3**a**), the NiAl sample shows two signals, both related to Ni reduction. The first peak with maximum around 390–400 °C is attributed to the reduction of surface NiO phase with no interaction with the mixed oxide or alumina, while the second reduction temperature is assigned to the reduction of Ni in strong interaction with the support [69]. Noteworthy, LDH decomposition also occurs currently to the reduction, producing CO_2 release [27]. On the other hand, it is possible to see that the ZnCuAl sample presents a more visible signal, corresponding to a reduction temperature of around 330 °C (onset at 263 °C), representative of the copper reduction, and a broader peak at higher temperatures probably due to the presence of bulk Cu species. Interestingly, when Ni and Cu are present in the same sample, a synergetic reduction is observed. In fact, NiCuAl sample shows an enhanced reducibility compared to the ZnCuAl and NiAl LDHs. The sample display a sharp peak shifted towards lower temperatures, related to reducible Ni and Cu species and a broader one at higher temperatures related to the reduction of bulk nickel. Noteworthy, the intensity of this broad band decreased while increasing the copper content in Ni/Cu samples indicating that nickel was already reduced at lower temperatures together with copper in this case. This behaviour can be assigned to hydrogen spill-over provided by copper that helps nickel reduction [70]. Moreover, increasing copper amount (NiCuAl 1.5:1.5:1) led to increased reducibility, with a peak maximum at 320 °C and an onset temperature at 240 °C. Indeed, the latter sample

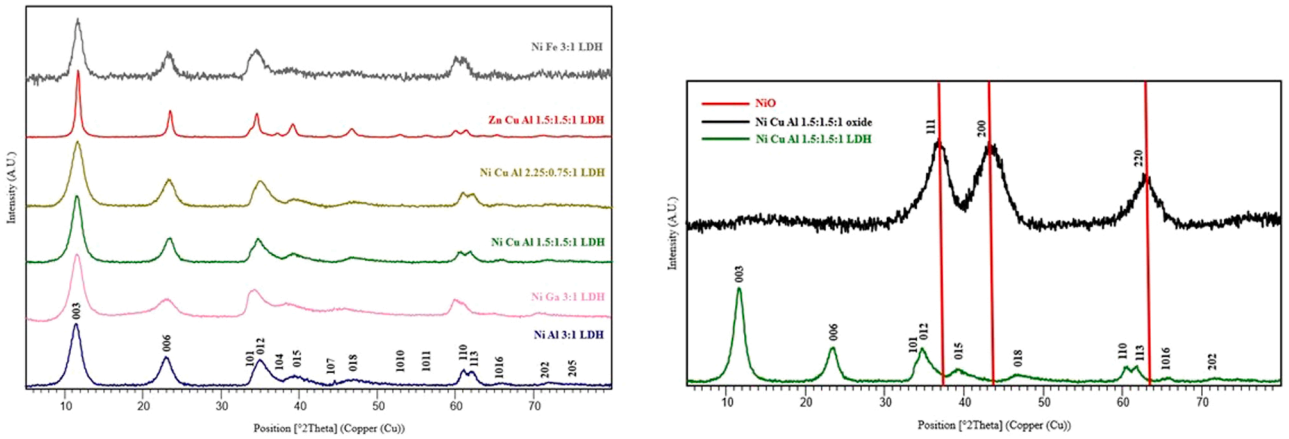

a. **b.**

Fig. 2. XRD patterns of LDH (a), and of NiCuAl 1.5:1.5:1 LDH and its respective oxide obtained after calcination (b).

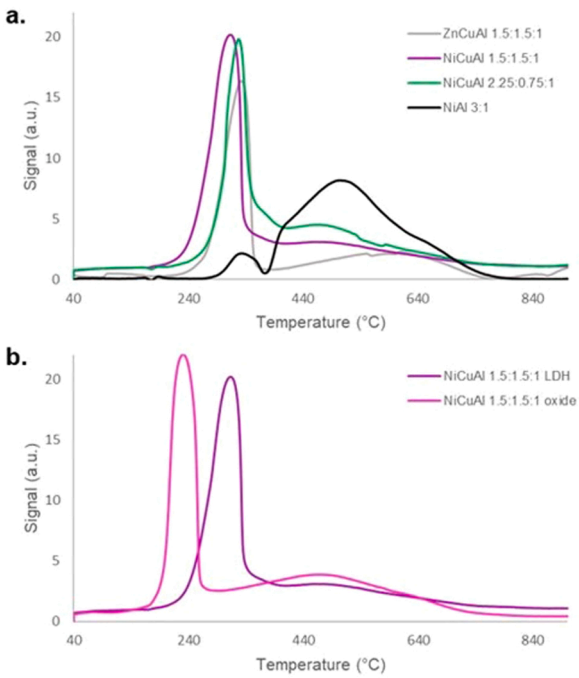

Fig. 3. TPR of (a) ZnCuAl 1.5:1.5:1, NiCuAl 1.5:1.5:1, NiCuAl 2.25:0.75:1, and NiAl 3:1 LDHs; (b) NiCuAl 1.5:1.5:1 LDH and oxide.

presents a main reduction peak at lower temperatures and a less intense shoulder, which indicates that a larger amount of bulk Cu and Ni has been already reduced at lower temperatures. This suggests a synergetic effect of Ni and Cu whose reducibility is increased when they are present in similar amounts. Sample reducibility was further increased by transforming the LDH into the corresponding mixed oxide (Fig. 3**b**). In fact, the calcined NiCuAl 1.5:1.5:1 sample showed a further decrease in reduction temperature with a shift of the peak maximum from 320 °C to around 210 °C and of the onset from 240 °C to 190 °C. This can be related to two different phenomena: first, the formation of a continuous 3D structure (mixed oxide) that allows for an easier charge delocalization through the oxide structure in contrast to the 2D-like LDH; second, the formation of the oxide allowed for the obtainment of smaller crystals with higher surface areas, as evidenced by XRD, which can increase the sample reducibility [68].

The NiCuAl 1.5:1.5:1 oxide, obtained by calcination of the corresponding LDH was further characterized by XPS, and the main results are reported in Fig. 4**a** and Table 2.

The Cu2p spectrum shows one peak at 933.43 eV which is assigned to $Cu(OH)_2$ specie accompanied by two satellite peaks at 943.69 eV and 940.42 eV. The first peak is usually observed at higher binding energy, 934.67 eV, as reported in literature [71]. The shift at lower binding energy suggests that the Cu is more electron-rich in the Ni-Cu mixed hydroxide phase. The shape of the satellite peaks, together with the ratio Cu/O of about 0.53 (Table 3), are consistent with the presence of Cu hydroxide phase on the catalyst surface. The Ni2p spectrum shows a peak at 855.94 eV attributed to a Ni^{2+} in the form of hydroxide phase [72] and it is accompanied by a satellite peak at 862.80 eV [72]. The Ni/O ratio of about 0.59 also supports this assignment. The O1s spectrum was deconvoluted in two main peaks. One component at 530.87 eV is assigned to -OH species while the second component at 532.12 eV represents Al-O species. This analysis shows that the surface of the LDH catalyst is predominantly a mixed hydroxide phase.

After the heating treatment, the XPS spectra were reported in Fig. 4**b** and Table 2. The Cu is present as Cu^{2+} in the form of CuO with the peak at 933.17 eV accompanied by two intense satellite peaks at 940.6 eV and 943.43 eV. The shift at lower binding energy of the Cu^{2+} peak agrees with the presence of Ni-Cu mixed oxide phase as observed in the LDH catalyst. The Ni2p spectra shows a main broader peak, and it is deconvoluted in three components. One at 856.57 eV assigned to a mixed Ni(II)/Ni(III) oxy-hydroxide phase, accompanied by two intense satellite peaks at 861.51 eV and 864.84 eV. The single peak at 854.87 eV

Table 2
Weight percentage (% w) of the species presents on the top-surface obtained by XPS analysis.

Sample	O1s (% w)	Al2p (% w)	Ni2p3 (% w)	Cu2p3 (% w)
LDH	36.64	22.53	21.51	19.32
Oxide	24.92	28.37	24.71	25.75

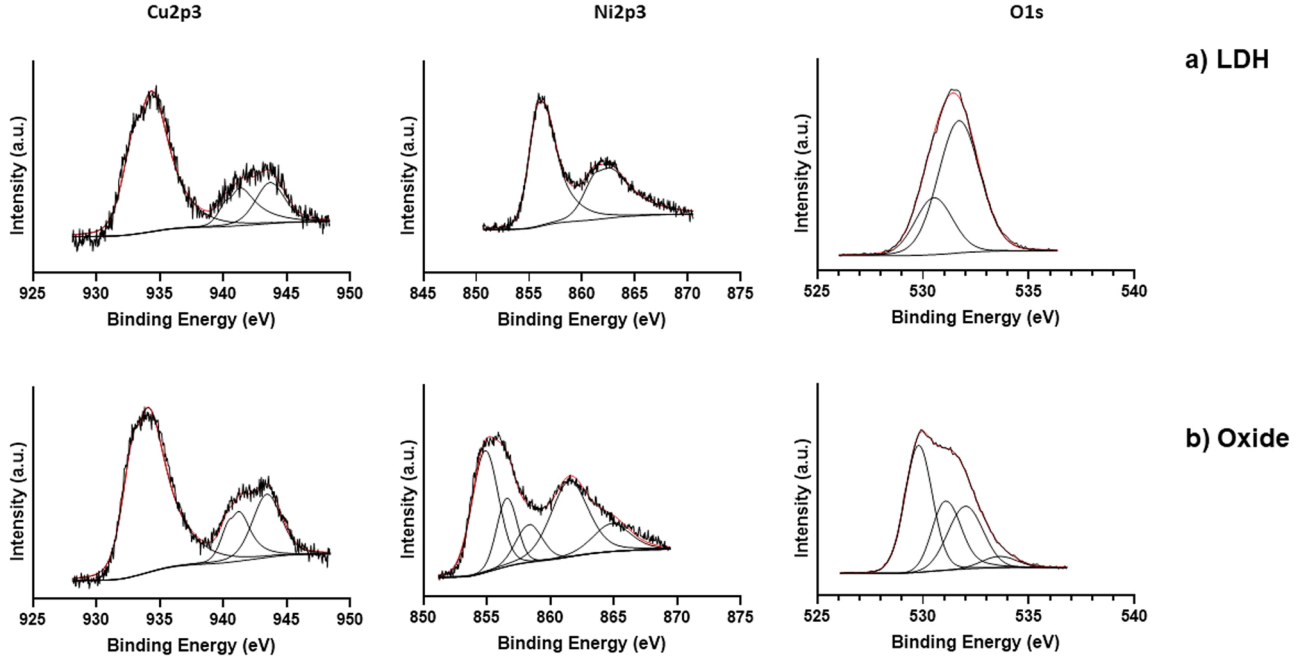

Fig. 4. XPS spectra of NiCuAl 1.5:1.5:1: a) LDH fresh b) oxide fresh.

Table 3
Weight Ratio of the species observed on the surface, by XPS analysis, for all the catalysts investigated.

Sample	Ni/Al	Cu/Al	Cu/Ni	Cu/O	Ni/O
LDH	0.95	0.86	0.90	0.53	0.59
Oxide	0.87	0.91	1.04	1.03	0.99

is attributed to NiO. Finally, an additional relatively minor component at 858.32 eV was attributed to Ni in mixed oxides. We could consider this component a Ni aluminate species at the interface between the particles and the support. This can be attributed to the higher affinity exhibited by Ni toward Al in respect to the activity it exhibited toward Cu [73]. It is important to note that all these peaks are slightly shifted at higher binding energies in respect to those observed in literature [74,75] suggesting that Ni is more electron deficient in the Ni-Cu mixed oxide phase. The O1s is deconvoluted in four components. One component at 529.80 eV is attributed to Ni-O [72]; the peaks at 531.06 eV and 532.01 eV are attributed to Cu-O and Al-O species, respectively. The small component at 533.62 eV is related to oxygen in Al–O or $NiAl_2O_4$ could be assigned to the metal that strongly interacts with oxygen as in the $NiAl_2O_4$ species or to the adsorbed H_2O on the surface [76].

3.2. Catalytic activity

The catalytic performances of the samples were examined in 4NP reduction in the presence of an excess of $NaBH_4$, monitoring the reaction process through UV–vis absorption spectroscopy to assess the influence of different parameters on their catalytic activity, such as the nature of the M^{2+} and M^{3+} cation, the co-presence of Ni and Cu, the effect of calcination and of reaction operative conditions. When mixed with the $NaBH_4$ solution, the 4NP aqueous solution changes from light yellow to bright yellow due to the deprotonation of 4NP, of which corresponding absorption peak in the UV-Vis spectra can be easily detected at 400 nm. The reaction mixture eventually turns into a colourless solution after the reduction of the nitro group with a parallel decrease of the intensity of the peak at 400 nm. In the meantime, an absorption peak at 300 nm, corresponding to the amino phenolate molecule, begins to be visible in the UV-Vis spectra. Therefore, the absorbance at 400 nm in the UV–Vis spectra was used to calculate the conversion of 4NP during reaction (Fig. 5), since the catalysts do not interfere in the same absorption range.

3.2.1. Effect of the M^{3+} cation

At first, the effect of the trivalent cation on the catalytic activity in 4NP reduction was investigated by using Ni-based LDH with different co-cations, namely Fe^{3+}, Ga^{3+}, and Al^{3+}. Fig. 6 displays the catalytic performance of Ni-based LDHs. Based on the results reported in Table 4,

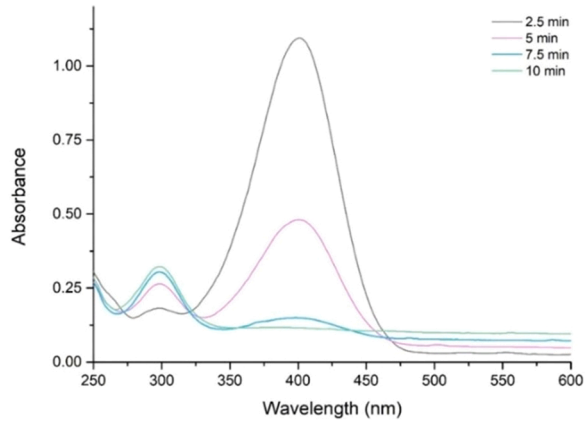

Fig. 5. Typical time-dependent evolution UV-Vis spectra during the catalytic reduction of 4NP.

the NiAl LDH showed the highest apparent constant (K_{app}), and therefore the greatest activity. Indeed, using this sample, a 75% conversion was reached in less than half time than its respective LDH with gallium and iron as trivalent cation. This is related to the higher surface area of the Al-containing sample, as suggested by the values of apparent kinetic constants normalized by the active area of the respective catalysts, which allowed for a higher contact between the substrate and the catalytic active sites, providing a faster conversion. Furthermore, the tests performed with pure alumina (Table 4), which showed no conversion, confirmed the crucial requirement of having a reducible divalent cation such as Ni in the catalyst structure. On the other hand, tests conducted with pure NiO also showed no activity, indicating that the mixed structure with interspersed Ni and Al cations has a crucial and positive role in 4NP reduction reaction and catalyst activation.

3.2.2. Effect of the copper and nickel presence

Having assessed the positive effect of Al^{3+} as trivalent cation and the necessity of the interspersed structure in 4NP reduction, the attention was shifted to the addition of another divalent cation (Cu^{2+}) to replace part of the Ni^{2+}, and able to cooperate with it in 4NP reduction. A series of samples containing different amounts of Cu^{2+} in the NiAl LDH framework, i.e., 0%, 25%, and 50%, (Cu/total Ni+Cu) was tested. A sample with a 100% Cu/total Ni+Cu, i.e., a CuAl sample was not prepared due to the challenges in preparing a homogeneous LDH containing a Cu^{2+}/M(II) higher than 1 without forming copper compounds with disordered octahedral sheets at the same time [27]. Thus, a ZnCuAl LDH with a M^{2+}/M^{3+} ratio of 3 and equal amounts of zinc and copper as M^{2+} was prepared and tested to show the catalytic activity of copper in the absence of nickel using Zn^{2+} as an inert M^{2+} cation that helped the inclusion of Cu^{2+} in the LDH framework. Fig. 7 shows the catalytic performances of the above discussed LDHs. The obtained results, reported in Table 5, show that adding Cu^{2+} in the Ni-based LDH structure increased the 4NP reduction. In particular, NiCuAl 1.5:1.5:1, which contained equal quantities of nickel and copper, showed a so fast conversion that it was not possible to calculate a kinetic constant for such tests using the same amount of catalyst used for other catalytic tests (10 mg), because nitrophenol was readily consumed before the first UV analysis, i.e., in less than 1 min of reaction. The sample not containing copper, NiAl and ZnCuAl, displayed the lowest apparent constants, evidencing how the co-presence of Ni and Cu significantly increases the reduction of 4NP. This was further evidenced by tests performed with pure NiO and CuO as catalysts. The results, reported in Table S1, have underlined that both catalysts' activities are way worse (even negligible in case of nickel oxide) when the Ni and Cu atoms are not present in the same structure.

In other words, copper sites alone in the LDH or oxide structure are not the key factors of fast nitrophenol reduction, but their co-presence with Ni in a high surface area structure is fundamental to increase the catalytic activity. This synergy was evidenced by TPR analysis, reported in Fig. 3. Indeed, both NiCuAl samples showed an enhanced reducibility compared to ZnCuAl and NiAl LDHs thanks to the hydrogen spill-over provided by copper presence which decreased the reduction onset temperature of about 20 °C and allowed for a homogeneous reduction, hence, supporting the results obtained during the 4NP reduction tests. This behaviour is more pronounced in the NiCuAl sample, where nickel and copper are present in a 1:1 ratio (NiCuAl 1.5:1.5:1). Furthermore, we can claim that the catalytic activities recorded for these samples are just slightly influenced by their surface area, as evidenced by the values of apparent kinetic constants normalized by the catalysts' active surface (Table 5); a further proof of the important role played by the presence of Ni and Cu sites in the material.

Therefore, from that moment onward, our study has been carried out with the aim of investigating other possible conditions able to further enhance the catalytic activity of the most promising sample, namely the NiCuAl 1.5:1.5:1 LDH.

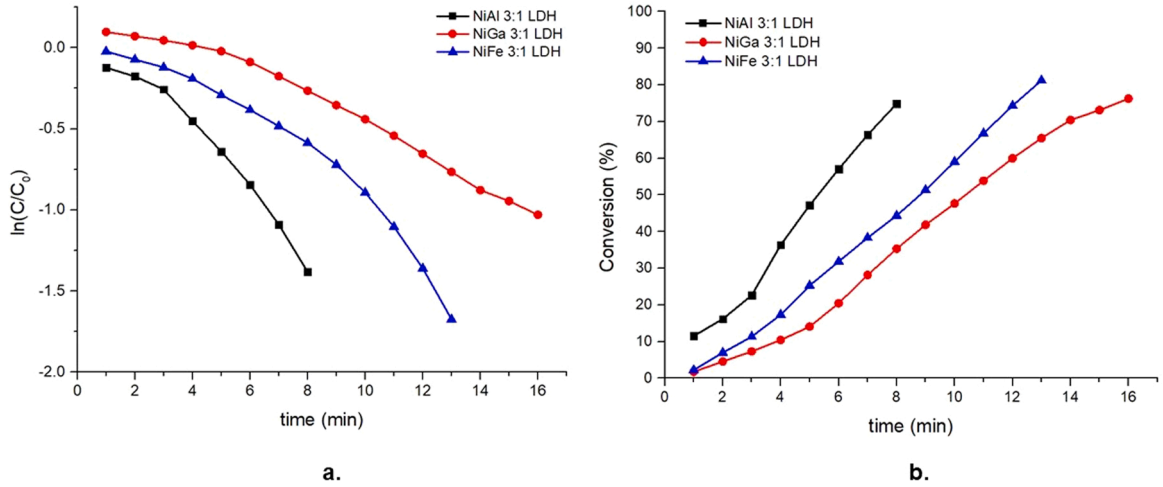

Fig. 6. Pseudo-first-order kinetic plot (a), and conversion plot (b) for the comparison of the activity of Ni-based LDH with different M^{3+} cations.

Table 4
Values of apparent constants for pseudo-first-order reactions using Ni-based LDH with different M^{3+} cations.

Sample	K_{app} (min^{-1})	K_{app} (min^{-1}/mg)	Active surface (m^2)	K_{app} (min^{-1}/m^2)
Ni Al 3:1	0.21 ± 0.02	**0.021 ± 0.002**	1.23	0.17 ± 0.02
Ni Ga 3:1	0.15 ± 0.07	**0.015 ± 0.007**	0.78	0.19 ± 0.07
Ni Fe 3:1	0.18 ± 0.06	**0.018 ± 0.006**	0.44	0.41 ± 0.06
Ni(II)O	0	**0**	-	0
Al_2O_3	0	**0**	-	0

3.2.3. *Effect of thermal treatment*

High surface area mixed oxides can be obtained by calcination of LDHs. In catalysis, layered-double hydroxides are mainly used after a calcination treatment which guarantees the synthesis of homogeneous mixed oxides. M^{2+} and M^{3+} LDH's cations are indeed able to rearrange in spinel phases ($M^{2+}(M^{3+})_2O_4$) above 750 °C and/or in a mixed M^{2+}/M^{3+} oxide structures with interspersed cations when the LDH is calcined between 350 and 700 °C [27,77,78]. The main benefits shown by the mixed oxides deriving from LDHs are their high surface areas, thermal stability and memory effect, i.e., the capability to reconstruct, under mild conditions in water solutions, the LDH structure.

The NiCuAl 1.5:1.5:1 LDH, i.e., the most performant LDH between the ones tested for the 4NP reduction reaction, has been subjected to a calcination at 400 °C to evaluate the effect of the structural change on the sample's catalytic activity.

The NiCuAl LDH and oxide catalysts have been tested in the 4NP reduction using, unlike before, 2 mg rather than 10 mg of catalyst to obtain a kinetic profile that could be monitored with our operando UV-Vis laboratory equipment. In fact, higher catalyst amount would lead to a total conversion in less than one minute of operation which does not allow drawing the kinetic behaviour of the catalyst, as mentioned in the previous Chapter. Fig. 8 shows the catalytic performance of the samples,

Table 5
Values of apparent constants for pseudo-first-order reactions using LDH with different M^{2+} cations.

Sample	K_{app} (min^{-1})	K_{app} (min^{-1}/mg)	Active surface (m^2)	K_{app} (min^{-1}/m^2)
Ni Al 3:1	0.21 ± 0.02	**0.021 ± 0.002**	1.23	0.17 ± 0.02
Ni Cu Al 1.5:1.5:1	**Too fast with 10 mg of catalyst**			
Ni Cu Al 2.25:0.75:1	0.65 ± 0.07	**0.065 ± 0.007**	1.03	0.63 ± 0.07
Zn Cu Al 1.5:1.5:1	0.13 ± 0.05	**0.013 ± 0.005**	0.60	0.22 ± 0.05

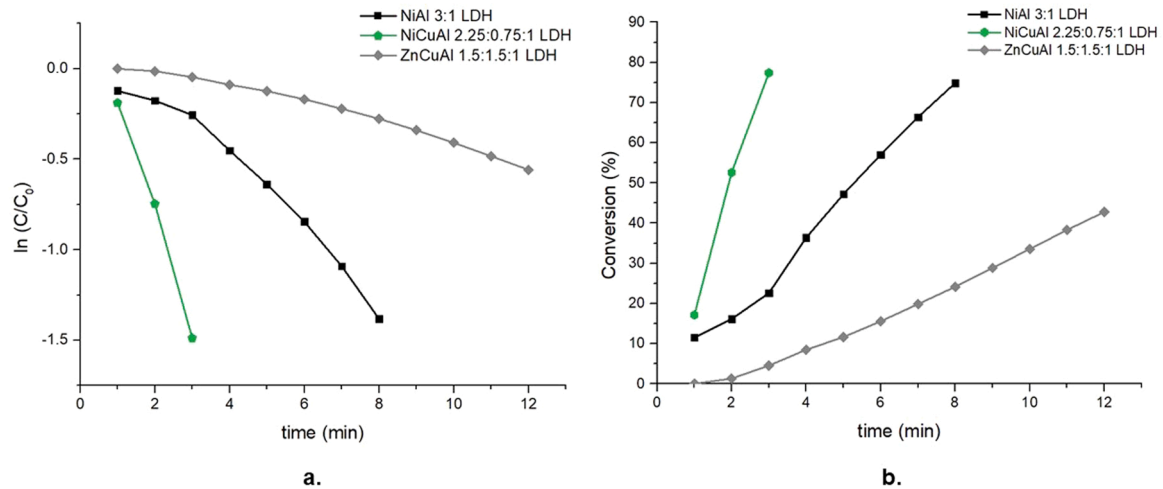

Fig. 7. Pseudo-first-order kinetic plot (a), and conversion plot (b) for the comparison of the activity of LDH with different M^{2+} cations.

while Table 6 reports the apparent kinetic constant relative to the two materials. First, it was possible to determine the apparent kinetic constant of the LDH material which was 0.61 min^{-1} under these conditions, while one of 1.06 min^{-1} has been observed for the oxide. The results showed that calcining the LDH to mixed oxide enhanced the catalyst's activity, as it can be concluded also by looking at the conversion plot. The enhanced activity of the oxide was related to the increased reducibility of the oxide with respect to the LDH, which has been confirmed by the TPR analysis, reported in Fig. 3, where both peak's maximum and onset temperatures are decreased by 110 °C and 50 °C respectively.

3.2.4. Effect of the catalyst amount

To evaluate the effect of the catalyst amount, the reaction has been conducted using 0.5, 1, and 2 mg of the same catalyst (NiCuAl 1.5:1.5:1 mixed oxide). As it is noticeable from Table 7 and Fig. S1 and S2, quadrupling the oxide amount led to an apparent rate constant enhanced by about five times (from 0.19 to 1.06 min^{-1}). Nevertheless, the non-linear relationship between the catalyst's amount and the reaction kinetic constant could be an indication of diffusion limitations phenomena, hence indicating that the reaction system is ruled by the presence of external mass transfer and kinetic regimes. The apparent kinetic constants found using the three different catalyst concentrations, were normalised by the mass of catalyst used and the average rate constant was found to be 0.5 ± 0.1 $min^{-1}mg^{-1}$. The not negligible standard deviation of K_{app} suggested again the presence of both kinetic and mass transfer regimes, and therefore, it can be claimed that the reaction efficiency could be further implemented by dealing with the mass transfer limitations and optimisation of reaction conditions (i.e., effect of stirring rate, 4NP concentration, amount of catalyst).

3.2.5. Effect of the reaction conditions

Reaction parameters have been investigated to reduce the effect of mass transfer. The first reaction parameter that has been studied has been the stirring rate, adding a magnetic stirrer inside the cuvette, in which 1 mg of catalyst has been placed, for all the reaction time.

As it is clear from Fig. 9, the catalyst's performances turned out to be further enhanced when an important stirring, of at least 1000 rpm, is applied to the reaction mixture. This outcome could be explained by a better miscibility between 4-nitrophenolate molecules and the more dispersed catalyst, that otherwise could settle at the bottom of the reaction vessel. By increasing the stirring rate between 500 and 1000 rpm, the rate of reaction increases, suggesting a region ruled by the presence of external mass transfer at low stirring rates. Stirring the reaction mixture in a range of 1000–1500 rpm is, on the other hand, the best condition to make the kinetic constant independent from the agitation speed as it is suggested by the constant K_{app} obtained under these conditions (Fig. S3).

Table 6
Values of apparent constants for pseudo-first-order reactions using NiCuAl 1.5:1.5:1 LDH and oxide.

Sample	K_{app} (min^{-1})	K_{app} (min^{-1}/mg)	Active surface (m^2)	K_{app} (min^{-1}/m^2)
Ni Cu Al 1.5:1.5:1 LDH	0.61 ± 0.02	**0.30 ± 0.01**	0.076	8.02
Ni Cu Al 1.5:1.5:1 oxide	1.06 ± 0.07	**0.53 ± 0.04**	0.12	8.83

Table 7
Values of apparent constants for pseudo-first-order reactions using NiCuAl 1.5:1.5:1 oxide in different amounts.

Sample	Catalyst amount (mg)	K_{app} (min^{-1})	K_{app} (min^{-1}/mg)
Ni Cu Al 1.5:1.5:1 oxide	0.5	0.19 ± 0.05	**0.38 ± 0.05**
Ni Cu Al 1.5:1.5:1 oxide	1	0.69 ± 0.05	**0.69 ± 0.05**
Ni Cu Al 1.5:1.5:1 oxide	2	1.06 ± 0.07	**0.53 ± 0.04**

3.2.6. Reusability tests

To complete the investigation on the NiCuAl 1.5:1.5:1 oxide catalyst, a reusability study was also conducted. The apparent kinetic constant and the conversion reached after a reaction time of 240 s have been used to compare the catalytic activity of the recycling tests. As reported in Fig. 10, the reaction rate constant, as well as the conversion, remained almost constant, considering the errors associated to the analyses. Furthermore, ICP analyses have been carried out on the reaction mixtures after removal of the catalyst to dispel any doubt about a possible nickel and/or copper leaching, which could have contributed to a decrease of activity, that, nonetheless, was not observed. No traces of the mentioned substances have been recorded. Thus, this result agrees with the stable activity of the catalyst during reusability tests.

3.2.7. Substituent effect and Hammett plot

To understand the structure correlation with the reactivity and the reduction mechanism, the substituent effect on different isomers of nitrophenol, namely, 2-, 3-, and 4-nitrophenol (Fig. 11) was studied during the catalytic tests involving the NiCuAl mixed oxide catalyst carrying out different tests using these three, respectively.

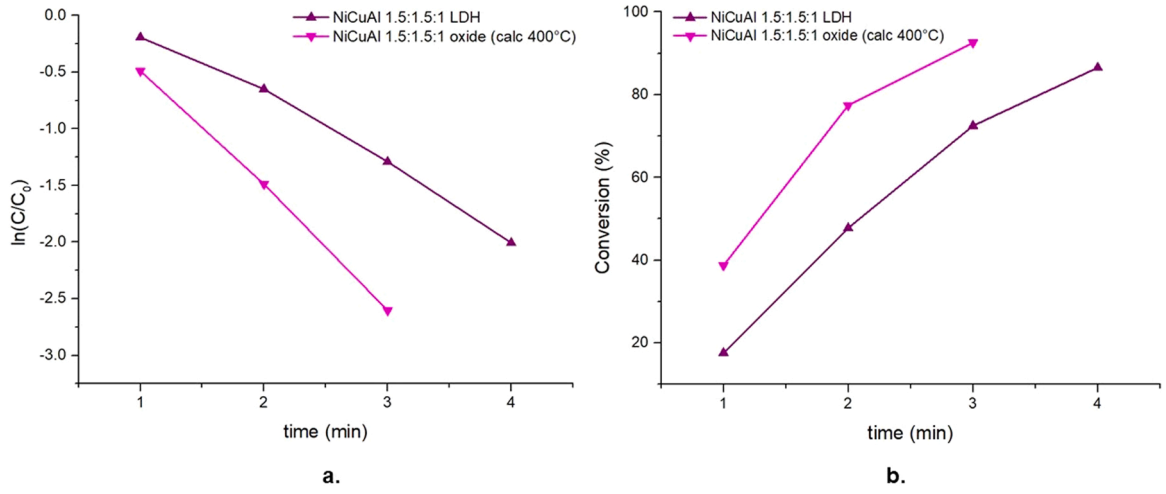

Fig. 8. Pseudo-first-order kinetic plot (a), and conversion plot (b) for the comparison of the activity of NiCuAl 1.5:1.5:1 LDH and oxide.

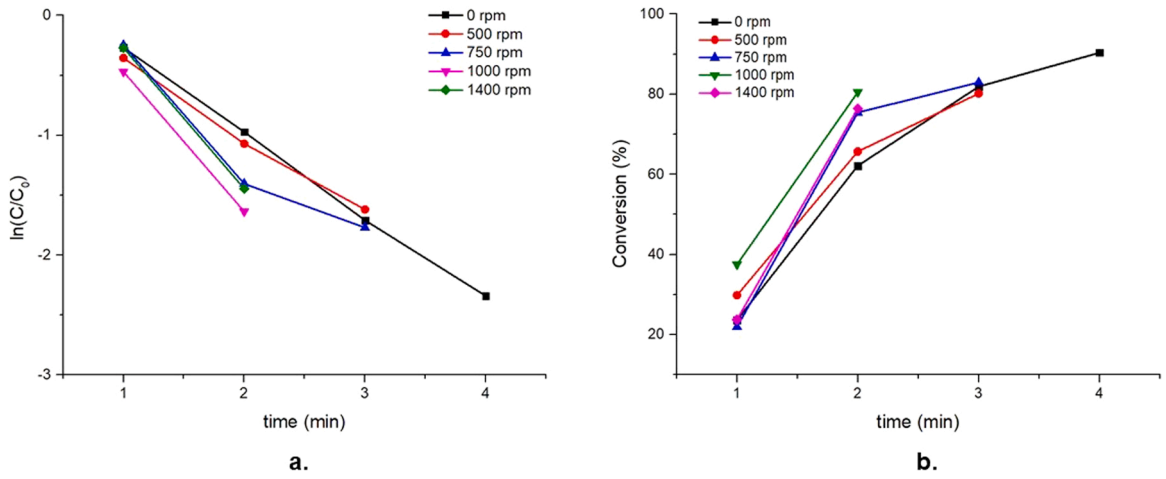

Fig. 9. Pseudo-first-order kinetic plot (a), and conversion plot (b) for the comparison of the activity of NiCuAl 1.5:1.5:1 oxide used at different stirring rate.

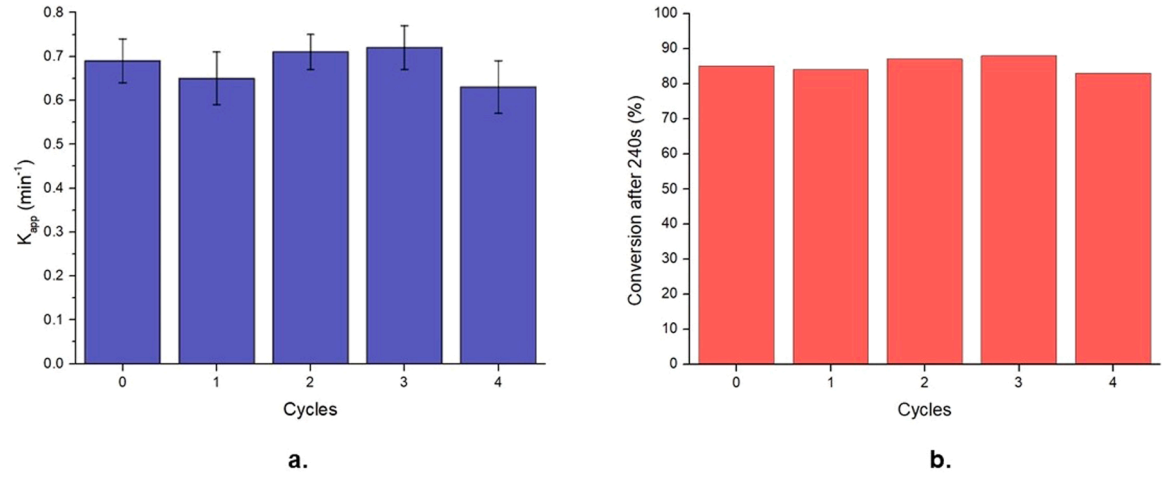

Fig. 10. - Plot of apparent kinetic constant (a) and conversion (b) per each run of the reusability tests performed with NiCuAl 1.5:1.5:1 oxide.

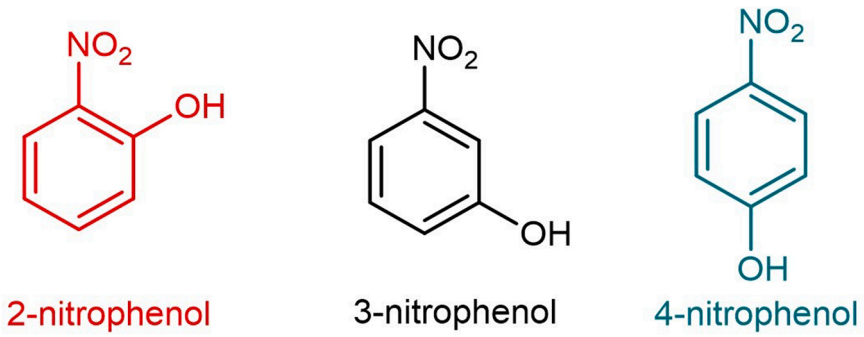

Fig. 11. 2-,3-, and 4-nitrophenol chemical structures.

The Hammett equation (Eq. 1) was used to understand the overall catalytic mechanism:

$$\log(K/K_0) = \sigma\rho \quad (1)$$

Where, K is the reaction equilibrium constant, K_0 is the reference reaction constant which considers a hydrogen atom as substituent of the phenol, σ is the substituent constant, and ρ the reaction constant [79]. This correlation gives indication about the effect of the electron-donating ability of the substituent group on the reaction kinetic constant. Indeed, the stability of the nitrophenolate ion, higher in the case of 2- and 4-NP, owing to the more resonance forms compared to 3-NP, affects the conversion rate of each isomer.

The results point out that the reaction rate obtained in the three tests with different nitrophenols, albeit showing in each case excellent results, is affected by the position of the substituent groups. Indeed, the Hammett plot shown in Fig. 12 indicates a good correlation between the revised σ values [80] and the reaction kinetic constants, with a positive slope (ρ= 0.18). This result confirms that the reaction rate is correlated to the electron-donating capacity and inductive effect associated with the substituents' position. Moreover, according to several studies found

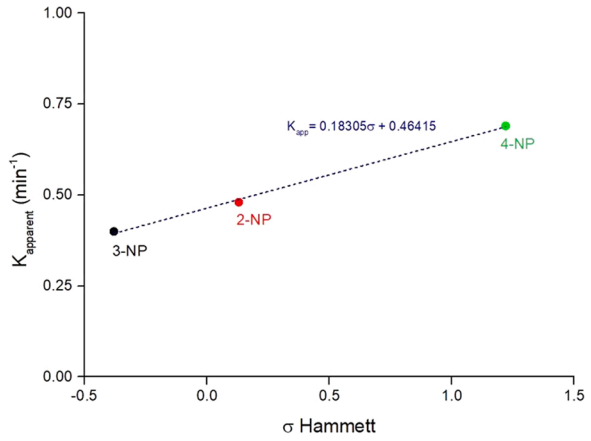

Fig. 12. Hammett plot for the effect of the substituent in NP isomers on the reaction rate. Reactions carried out using 25 mL of a $2{\cdot}10^{-4}$ M NP solution, 25 mL of a $9.0{\cdot}10^{-3}$ M $NaBH_4$ solution, and 1 mg of NiCuAl 1.5:1.5:1 oxide as catalyst.

in the literature which thoroughly investigates the possible reaction routes through KIE studies supported by NMR spectroscopy, our Hammett kinetics sustains the observation of a negative charge, or hydride transfer, in the transition state of the reaction, stabilised by the electron-withdrawing groups [13,79,81].

Indeed, the rate of reduction for the different substrates follows the order 4NP > 2NP > 3NP, namely the reaction proceeds faster as the electron-donating ability of the substituent group increases (Table S2).

To conclude the study, the results obtained in this work were compared with what has been reported in the literature. Our best catalyst (NiCuAl 1.5:1.5:1 oxide) was able to perform at the level of the already reported best ones with K_{app} value of $1.2{\cdot}10^{-2}$ s^{-1}/mg, as it is shown in Table S3. It is worth noticing that, in contrast to the other materials employed nowadays in 4-nitrophenol conversion, the catalyst optimised in this work is not made of noble metals (such as gold, palladium, or platinum), it is not supported by any other materials, and, finally, it is obtained with an easy and economic preparation technique. All these benefits should be added to the already remarkable performances that the oxide has shown during the tests, which can be considered comparable or even higher than the ones reported in the literature.

3.3. Characterization of the spent catalyst

To better understand the catalysts behaviour during reaction, in-depth analyses on the spent (used) mixed oxide have been carried out. Interestingly, as reported in Fig. S4b, the XRD of the spent NiCuAl 1.5:1.5:1 oxide highlighted the presence of two more phases as compared to the fresh catalyst (Fig. S4a), i.e., a nickel aluminate phase and a CuO phase. This change in the active phase structure could be explained by a migration of copper atoms towards the catalyst surface during reaction which, after air exposure, rapidly oxidise. Therefore, thanks to the well-known affinity of metallic copper and CuO for nitro group reductions [82–84], the just described behaviour involving the formation of metallic copper over the catalyst surface during 4NP reduction could represent the key aspect of this catalyst's remarkable activity in the reduction of 4NP to 4AP.

XPS analysis was further used to confirm this hypothesis by monitoring the oxidation state of the catalysts after the catalytic tests and comparing them with the XPS results obtained on the as-synthesized (fresh) catalysts.

The XPS analyses of the spent catalysts are similar to those obtained for the fresh ones, except for the Cu2p spectra, reported in Fig. S5. Two main observations can be made: (i) the satellite peak is less intense in respect to the fresh one (Fig. S5b) and the main peak at 932.85 eV is shifted to a lower binding energy in respect to that observed in the fresh sample, 933.17 eV, suggesting that the metallic Cu could be formed during the reaction since an excess of $NaBH_4$ has been used and $NaBH_4$ is a strong reducing agent and, thus, it can migrate toward the top surface layer of the catalyst. Moreover, the O1s spectrum of the spent oxide catalyst exhibits an increase of the component assigned to Ni-O (529.80 eV), while, on the contrary, the one assigned to Cu-O (531.06 eV) decreases, highlighting that part of copper oxide could be reduced and migrate toward the top-surface. The weight percentage of all the species analysed by XPS are reported in Table S4. By comparing the LDH before and after the test, a similar amount of Cu and Ni, about 2% weight, migrates toward the top surface. Concerning the oxide sample, the Ni that interacts more strongly with Al in respect to the Cu does not migrate, maintaining the same amount of weight, about 24%, in both fresh and spent catalysts. On the other hand, the Cu slightly migrates toward the top surface passing from 25.75% to 26.40% after reaction. These results support the surface enrichment of copper in presence of $NaBH_4$, that could be reduced to metallic copper favouring the migration toward the surface, and hence facilitating the reduction of 4NP. A further confirmation of the copper migration towards the surface has been shown by TEM analysis. The spent sample, illustrated in Fig. 13, shows the presence of Cu_2O nanoparticles over the surface, as confirmed by EDS and SAED analysis. Indeed, on the one hand, EDS analysis shows that these particles are only composed of copper, which has segregated as metallic copper from the NiCuAl mixed oxide. However, these small metallic clusters are readily oxidized in air, as suggested indeed by the results of SAED which show a d-spacing of 2.42 Å, characteristic of Cu_2O. Furthermore, it is worth mentioning that a possible reactivation of the oxidized copper, performed for instance through a further in situ reduction with $NaBH_4$ before a second reduction cycle, could benefit the reaction performances by restoring the actual active sites, i.e., metallic Cu. In fact, the results of the recycling tests, where stable conversion has been obtained over different repetitions, suggest that the copper oxide is readily reduced to metal when an excess of $NaBH_4$ is present in the reaction environment, restoring the catalytic activity.

4. Conclusions

A series of LDHs with intercalated carbonates were synthetized following a co-precipitation method for the 4-nitrophenol to 4-aminophenol reduction reaction varying the catalyst composition. XRD, TPR, BET-surface area, XPS, and TEM analysis were carried out to study the structural and morphological properties of the prepared catalysts and propose structure-activity relationships.

Aluminium was identified as the best trivalent cation if compared to Ga- or Fe-based LDHs, an outcome related to the higher surface area of the Al-containing sample, which facilitates the substrate/active site contact and, hence, the 4NP conversion.

Furthermore, a Ni/Cu synergetic effect was highlighted and confirmed by means of TPR, XPS, and direct comparison with nickel and copper containing catalysts. Catalytic performance has shown to be further increased by calcination at 400 °C of the NiCuAl LDH to mixed oxide.

The results obtained in this study demonstrate that NiCuAl-based mixed oxide derived from LDH, in which nickel divalent cations are partially substituted with copper, are promising catalysts for 4NP reduction reactions. This remarkable behaviour has been explained and proven, through XPS and TEM analyses, by the migration of copper atoms towards the catalyst surface.

By varying the experimental parameters, it was possible to determine the optimal reaction conditions (i.e., a stirring rate of at least 1000 rpm), as well as the main challenges to overcome, such as the reaction rate's dependence on mass transfer.

The effect of substituents on the aromatic ring of the substrate was

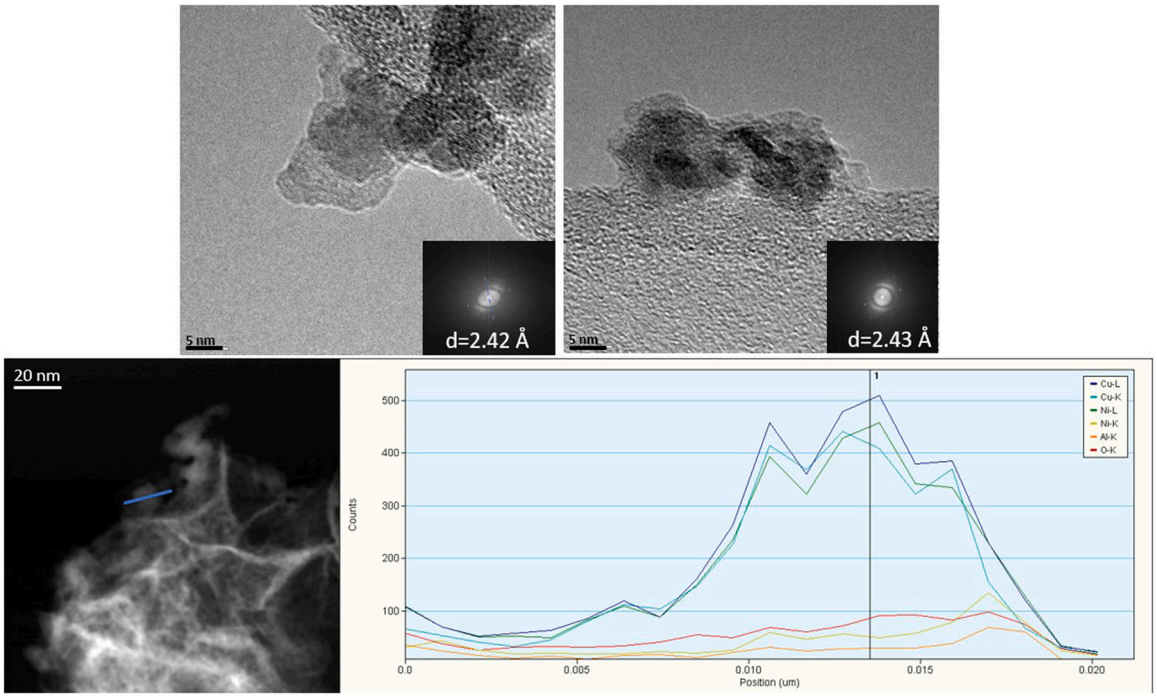

Fig. 13. TEM, STEM and EDS analysis of the spent NiCuAl 1.5:.15:1 mixed oxide.

studied and the Hammett equation was used to deepen the reaction mechanism. 4NP was found the most reactive isomer due to its higher stability once deprotonated. Besides, being a reaction linked to the electron-donating capacity and inductive effect associated with the substituents' position, the Hammett plot showed the possibility of having a negative charge, or hydride transfer, in the transition state of the reaction, stabilised by the electron-withdrawing groups.

Finally, the catalyst was found to be stable as recycling tests showed constant reaction conversion after repeated cycles.

CRediT authorship contribution statement

E. Orfei: Conceptualization, Data curation, Formal analysis, Methodology, Validation, Visualization, Writing – review & editing. **A. Fasolini**: Supervision, Conceptualization, Data curation, Formal analysis, Methodology, Validation, Writing – review & editing. **S. Abate**: Conceptualization, data curation, formal analysis, validation, review, and editing. **N. Dimitratos**: supervision, conceptualization, Formal analysis, Wriing – review & editing. **F. Basile**: Supervision, Conceptualization, Formal analysis, Project administration, Writing – review & editing. All authors have read and agreed to the published version of the manuscript.

Declaration of Competing Interest

The authors declare that they have no known competing financial interests or personal relationships that could have appeared to influence the work reported in this paper.

Data availability

Data will be made available on request.

Acknowledgements

This research did not receive any specific grant from funding agencies in the public, commercial, or not-for-profit sectors.

Appendix A. Supporting information

Supplementary data associated with this article can be found in the online version at doi:10.1016/j.cattod.2023.114153.

References

[1] J. Fu, S. Wang, J. Zhu, K. Wang, M. Gao, X. Wang, Q. Xu, Au-Ag bimetallic nanoparticles decorated multi-amino cyclophosphazene hybrid microspheres as enhanced activity catalysts for the reduction of 4-nitrophenol, Mater. Chem. Phys. 207 (2018) 315–324, https://doi.org/10.1016/j.matchemphys.2018.01.002.
[2] M. Muniz-Miranda, SERS monitoring of the catalytic reduction of 4-nitrophenol on Ag-doped titania nanoparticles, Appl. Catal. B Environ. 146 (2014) 147–150, https://doi.org/10.1016/j.apcatb.2013.03.008.
[3] S.M. Rogers, C.R.A. Catlow, D. Gianolio, P.P. Wells, N. Dimitratos, Supported metal nanoparticles with tailored catalytic properties through sol-immobilisation: applications for the hydrogenation of nitrophenols, Faraday Discuss. 208 (2018) 443–454, https://doi.org/10.1039/C7FD00216E.
[4] B. Pan, W. Du, W. Zhang, X. Zhang, Q. Zhang, B. Pan, L. Lv, Q. Zhang, J. Chen, Improved adsorption of 4-nitrophenol onto a novel hyper-cross-linked polymer, Environ. Sci. Technol. 41 (2007) 5057–5062, https://doi.org/10.1021/es070134d.
[5] K. Alshammari, Y. Niu, R.E. Palmer, N. Dimitratos, Optimization of sol-immobilized bimetallic Au–Pd/TiO2 catalysts: reduction of 4-nitrophenol to 4-aminophenol for wastewater remediation, Philos. Trans. R. Soc. A Math. Phys. Eng. Sci. 378 (2020), 20200057, https://doi.org/10.1098/rsta.2020.0057.
[6] MarinelL. Farré, A. Oubiña, M.P. Marco, A. Ginebreda, L. Tirapu, D. Barceló, Evaluation of 4-nitrophenol elisa kit for assessing the origin of organic pollution in wastewater treatment works, Environ. Sci. Technol. 33 (1999) 3898–3904, https://doi.org/10.1021/es990402a.
[7] M.C. Tomei, M.C. Annesini, R. Luberti, G. Cento, A. Senia, Kinetics of 4-nitrophenol biodegradation in a sequencing batch reactor, Water Res. 37 (2003) 3803–3814, https://doi.org/10.1016/S0043-1354(03)00297-5.
[8] T. Aditya, J. Jana, N.K. Singh, A. Pal, T. Pal, Remarkable facet selective reduction of 4-nitrophenol by morphologically tailored (111) faceted Cu $_2$ O Nanocatalyst, ACS Omega 2 (2017) 1968–1984, https://doi.org/10.1021/acsomega.6b00447.
[9] R. Djellabi, R. Giannantonio, E. Falletta, C.L. Bianchi, SWOT analysis of photocatalytic materials towards large scale environmental remediation, Curr. Opin. Chem. Eng. 33 (2021), 100696, https://doi.org/10.1016/j.coche.2021.100696.
[10] S. Wunder, Y. Lu, M. Albrecht, M. Ballauff, Catalytic activity of faceted gold nanoparticles studied by a model reaction: evidence for substrate-induced surface restructuring, ACS Catal. 1 (2011) 908–916, https://doi.org/10.1021/cs200208a.
[11] S. Wunder, F. Polzer, Y. Lu, Y. Mei, M. Ballauff, Kinetic analysis of catalytic reduction of 4-nitrophenol by metallic nanoparticles immobilized in spherical polyelectrolyte brushes, J. Phys. Chem. C 114 (2010) 8814–8820, https://doi.org/10.1021/jp101125j.

[12] J. Strachan, C. Barnett, A.F. Masters, T. Maschmeyer, 4-nitrophenol reduction: probing the putative mechanism of the model reaction, ACS Catal. 10 (2020) 5516–5521, https://doi.org/10.1021/acscatal.0c00725.

[13] S. Fountoulaki, V. Daikopoulou, P.L. Gkizis, I. Tamiolakis, G.S. Armatas, I. N. Lykakis, Mechanistic studies of the reduction of nitroarenes by nabh4 or hydrosilanes catalyzed by supported gold nanoparticles, ACS Catal. 4 (2014) 3504–3511, https://doi.org/10.1021/cs500379u.

[14] P. Zhao, X. Feng, D. Huang, G. Yang, D. Astruc, Basic concepts and recent advances in nitrophenol reduction by gold- and other transition metal nanoparticles, Coord. Chem. Rev. 287 (2015) 114–136, https://doi.org/10.1016/j.ccr.2015.01.002.

[15] S. Cattaneo, S. Althahban, S.J. Freakley, M. Sankar, T. Davies, Q. He, N. Dimitratos, C.J. Kiely, G.J. Hutchings, Synthesis of highly uniform and composition-controlled gold-palladium supported nanoparticles in continuous flow, Nanoscale 11 (2019) 8247–8259, https://doi.org/10.1039/C8NR09917K.

[16] L. Abis, S.J. Freakley, G. Dodekatos, D. Morgan, M. Sankar, N. Dimitratos, Q. He, C. Kiely, G. Hutchings, Highly active gold and gold-palladium catalysts prepared by colloidal methods in the absence of polymer stabilizers, ChemCatChem 9 (2017) 2914–2918, https://doi.org/10.1002/cctc.201700483.

[17] J. Singh, A. Mehta, M. Rawat, S. Basu, Green synthesis of silver nanoparticles using sun dried tulsi leaves and its catalytic application for 4-nitrophenol reduction, J. Environ. Chem. Eng. 6 (2018) 1468–1474, https://doi.org/10.1016/j.jece.2018.01.054.

[18] A. Mehta, M. Sharma, A. Kumar, S. Basu, Gold nanoparticles grafted mesoporous silica: a highly efficient and recyclable heterogeneous catalyst for reduction of 4-nitrophenol, Nano 11 (2016), https://doi.org/10.1142/S1793292016501046.

[19] B. Acosta, V. Evangelista, S. Miridonov, S. Fuentes, A. Simakov, The decoration of gold core in au@zro2 nanoreactors with trace amounts of pd for the effective reduction of 4-nitrophenol to 4-aminophenol, Catal. Lett. 149 (2019) 1621–1632, https://doi.org/10.1007/s10562-019-02758-y.

[20] I.T. Papadas, S. Fountoulaki, I.N. Lykakis, G.S. Armatas, Controllable synthesis of mesoporous iron oxide nanoparticle assemblies for chemoselective catalytic reduction of nitroarenes, Chem. A Eur. J. 22 (2016) 4600–4607, https://doi.org/10.1002/chem.201504685.

[21] E. Vasilikogiannaki, C. Gryparis, V. Kotzabasaki, I.N. Lykakis, M. Stratakis, Facile reduction of nitroarenes into anilines and nitroalkanes into hydroxylamines via the rapid activation of ammonia·borane complex by supported gold nanoparticles, Adv. Synth. Catal. 355 (2013) 907–911, https://doi.org/10.1002/adsc.201200983.

[22] M. López-Cisneros, E. Smolentseva, B. Acosta, A. Simakov, Synthesis by spray pyrolysis of gold nano species confined in iron oxide nanospheres effective in the reduction of 4-nitrophenol to 4-aminophenol, Nanotechnology 32 (2021), https://doi.org/10.1088/1361-6528/ac137c.

[23] G. García-Valdivieso, E. Arenas-Sánchez, P. Horta-Fraijo, A. Simakov, H. R. Navarro-Contreras, B. Acosta, Ag@ZnO/MWCNT ternary nanocomposite as an active and stable catalyst for the 4-nitrophenol reduction in water, Nanotechnology 32 (2021), https://doi.org/10.1088/1361-6528/abf96b.

[24] P. Horta-Fraijo, E. Smolentseva, A. Simakov, M. José-Yacaman, B. Acosta, Ag nanoparticles in A4 zeolite as efficient catalysts for the 4-nitrophenol reduction, Microporous Mesoporous Mater. 312 (2021), https://doi.org/10.1016/j.micromeso.2020.110707.

[25] N. Arora, A. Mehta, A. Mishra, S. Basu, 4-Nitrophenol reduction catalysed by Au-Ag bimetallic nanoparticles supported on Ldh: homogeneous vs. heterogeneous catalysis, Appl. Clay Sci. 151 (2018) 1–9, https://doi.org/10.1016/j.clay.2017.10.015.

[26] J. Zhou, X. Liu, J. Huang, D. Guo, H. Sun, C. Xu, J. Zhang, X. Ji, J. Ma, L. Liu, Z. Tong, Construction of novel Ag@SrNbO/LDH ternary hybrid with high catalytic performance towards the reduction of 4-nitrophenol, Appl. Surf. Sci. 581 (2022), 152425, https://doi.org/10.1016/j.apsusc.2022.152425.

[27] F. Cavani, F. Trifirò, A. Vaccari, Hydrotalcite-type anionic clays: preparation properties and applications, Catal. Today 11 (1991) 173–301, https://doi.org/10.1016/0920-5861(91)80068-K.

[28] P.S. Jijoe, S.R. Yashas, H.P. Shivaraju, Fundamentals synthesis characterization and environmental applications of layered double hydroxides: a review, Environ. Chem. Lett. (2021), https://doi.org/10.1007/s10311-021-01200-3.

[29] J. De Maron, M. Eberle, F. Cavani, F. Basile, N. Dimitratos, P.J. Maireles-Torres, E. Rodriguez-Castellón, T. Tabanelli, Continuous-flow methyl methacrylate synthesis over gallium-based bifunctional catalysts, ACS Sustain. Chem. Eng. 9 (2021) 1790–1803, https://doi.org/10.1021/acssuschemeng.0c07932.

[30] N. Baig, M. Sajid, Applications of layered double hydroxides based electrochemical sensors for determination of environmental pollutants: a review, Trends Environ. Anal. Chem. 16 (2017) 1–15, https://doi.org/10.1016/j.teac.2017.10.003.

[31] A. Faour, C. Mousty, V. Prevot, B. Devouard, A. De Roy, P. Bordet, E. Elkaim, C. Taviot-Gueho, Correlation among structure microstructure and electrochemical properties of nial–co3 layered double hydroxide thin films, J. Phys. Chem. C. 116 (2012) 15646–15659, https://doi.org/10.1021/jp300780w.

[32] J. Hynek, J. Rathouský, J. Demel, K. Lang, Design of porphyrin-based conjugated microporous polymers with enhanced singlet oxygen productivity, RSC Adv. 6 (2016) 44279–44287, https://doi.org/10.1039/C6RA04066G.

[33] A. Fasolini, S. Abate, D. Barbera, G. Centi, F. Basile, Pure H2 production by methane oxy-reforming over Rh-Mg-Al hydrotalcite-derived catalysts coupled with a Pd membrane, Appl. Catal. A Gen. 581 (2019) 91–102, https://doi.org/10.1016/j.apcata.2019.05.024.

[34] A. Fasolini, D. Cespi, T. Tabanelli, R. Cucciniello, F. Cavani, Hydrogen from renewables: a case study of glycerol reforming, Catalysts 9 (2019) 722, https://doi.org/10.3390/catal9090722.

[35] A. Fasolini, R. Cucciniello, E. Paone, F. Mauriello, T. Tabanelli, A short overview on the hydrogen production via aqueous phase reforming (APR) of cellulose C6-C5 sugars and polyols, Catalysts 9 (2019) 917.

[36] N. Dewangan, W.M. Hui, S. Jayaprakash, A.-R. Bawah, A.J. Poerjoto, T. Jie, A. Jangam, K. Hidajat, S. Kawi, Recent progress on layered double hydroxide (LDH) derived metal-based catalysts for CO_2 conversion to valuable chemicals, Catal. Today 356 (2020) 490–513, https://doi.org/10.1016/j.cattod.2020.06.020.

[37] J. Qu, L. Sha, C. Wu, Q. Zhang, Applications of mechanochemically prepared layered double hydroxides as adsorbents and catalysts: a mini-review, Nanomaterials 9 (2019) 80, https://doi.org/10.3390/nano9010080.

[38] G. Fan, F. Li, D.G. Evans, X. Duan, Catalytic applications of layered double hydroxides: recent advances and perspectives, Chem. Soc. Rev. 43 (2014) 7040–7066, https://doi.org/10.1039/C4CS00160E.

[39] N. Schiaroli, C. Lucarelli, M.C. Iapalucci, G. Fornasari, A. Crimaldi, A. Vaccari, Combined reforming of clean biogas over nanosized ni–rh bimetallic clusters, Catalysts 10 (2020) 1345, https://doi.org/10.3390/catal10111345.

[40] T. Tabanelli, S. Cocchi, B. Gumina, L. Izzo, M. Mella, S. Passeri, F. Cavani, C. Lucarelli, J. Schütz, W. Bonrath, T. Netscher, Mg/Ga mixed-oxide catalysts for phenol methylation: outstanding performance in 2,4,6-trimethylphenol synthesis with co-feeding of water, Appl. Catal. A Gen. 552 (2018) 86–97, https://doi.org/10.1016/j.apcata.2018.01.001.

[41] T. Tabanelli, Unrevealing the hidden link between sustainable alkylation and hydrogen transfer processes with alcohols, Curr. Opin. Green. Sustain. Chem. 29 (2021), 100449, https://doi.org/10.1016/j.cogsc.2021.100449.

[42] Y. Izumi, Recent advances in the photocatalytic conversion of carbon dioxide to fuels with water and/or hydrogen using solar energy and beyond, Coord. Chem. Rev. 257 (2013) 171–186, https://doi.org/10.1016/j.ccr.2012.04.018.

[43] J. Ran, M. Jaroniec, S.-Z. Qiao, Cocatalysts in semiconductor-based photocatalytic co2 reduction: achievements, challenges, and opportunities, Adv. Mater. 30 (2018), 1704649, https://doi.org/10.1002/adma.201704649.

[44] K. Teramura, S. Iguchi, Y. Mizuno, T. Shishido, T. Tanaka, Photocatalytic conversion of co2 in water over layered double hydroxides, Angew. Chem. Int. Ed. 51 (2012) 8008–8011, https://doi.org/10.1002/anie.201201847.

[45] Z. Yang, F. Wang, C. Zhang, G. Zeng, X. Tan, Z. Yu, Y. Zhong, H. Wang, F. Cui, Utilization of ldh-based materials as potential adsorbents and photocatalysts for the decontamination of dyes wastewater: a review, RSC Adv. 6 (2016) 79415–79436, https://doi.org/10.1039/C6RA12727D.

[46] Z. Yang, C. Zhang, G. Zeng, X. Tan, D. Huang, J. Zhou, Q. Fang, K. Yang, H. Wang, J. Wei, K. Nie, State-of-the-art progress in the rational design of layered double hydroxide based photocatalysts for photocatalytic and photoelectrochemical H2/O2 production, Coord. Chem. Rev. 446 (2021), 214103, https://doi.org/10.1016/j.ccr.2021.214103.

[47] G. Zhao, J. Zou, X. Chen, J. Yu, F. Jiao, Layered double hydroxides materials for photo(electro-) catalytic applications, Chem. Eng. J. 397 (2020), 125407, https://doi.org/10.1016/j.cej.2020.125407.

[48] X. Bian, S. Zhang, Y. Zhao, R. Shi, T. Zhang, Layered double hydroxide-based photocatalytic materials toward renewable solar fuels production, InfoMat 3 (2021) 719–738, https://doi.org/10.1002/inf2.12192.

[49] H. Boumeriame, E.S. Da Silva, A.S. Cherevan, T. Chafik, J.L. Faria, D. Eder, Layered double hydroxide (LDH)-based materials: a mini-review on strategies to improve the performance for photocatalytic water splitting, J. Energy Chem. 64 (2022) 406–431, https://doi.org/10.1016/j.jechem.2021.04.050.

[50] A. Razzaq, S. Ali, M. Asif, S.-I. In, Layered double hydroxide (ldh) based photocatalysts: an outstanding strategy for efficient photocatalytic co2 conversion, Catalysts 10 (2020) 1185, https://doi.org/10.3390/catal10101185.

[51] L. Mohapatra, K. Parida, A review on the recent progress challenges and perspective of layered double hydroxides as promising photocatalysts, J. Mater. Chem. A 4 (2016) 10744–10766, https://doi.org/10.1039/C6TA01668E.

[52] A. Laskowska, Z.M.G. Boiteux, O. Gain, A. Marzec, W. Maniukiewicz, Ionic elastomers based on carboxylated nitrile rubber (xnbr) and magnesium aluminum layered double hydroxide, EXPRESS Polym. Lett. 8 (2014) 374–386, https://doi.org/10.3144/expresspolymlett.2014.42.

[53] Z. Lü, F. Zhang, X. Lei, L. Yang, S. Xu, X. Duan, In situ growth of layered double hydroxide films on anodic aluminum oxide/aluminum and its catalytic feature in aldol condensation of acetone, Chem. Eng. Sci. 63 (2008) 4055–4062, https://doi.org/10.1016/j.ces.2008.05.007.

[54] N. Schiaroli, M. Volanti, A. Crimaldi, F. Passarini, A. Vaccari, G. Fornasari, S. Copelli, F. Florit, C. Lucarelli, Biogas to syngas through the combined steam/dry reforming process: an environmental impact assessment, Energy Fuels 35 (2021) 4224–4236, https://doi.org/10.1021/acs.energyfuels.0c04066.

[55] P. Tarifa, N. Schiaroli, P.H. Ho, F. Cañaza, F. Ospitali, G. Sanghez de Luna, C. Lucarelli, G. Fornasari, A. Vaccari, A. Monzon, P. Benito, Steam reforming of clean biogas over Rh and Ru open-cell metallic foam structured catalysts, Catal. Today 383 (2022) 74–83, https://doi.org/10.1016/j.cattod.2021.03.024.

[56] S. Xu, S. Chansai, Y. Shao, S. Xu, Y. Wang, S. Haigh, Y. Mu, Y. Jiao, C.E. Stere, H. Chen, X. Fan, C. Hardacre, Mechanistic study of non-thermal plasma assisted CO_2 hydrogenation over Ru supported on MgAl layered double hydroxide, Appl. Catal. B Environ. 268 (2020), 118752, https://doi.org/10.1016/j.apcatb.2020.118752.

[57] G. Chen, R. Gao, Y. Zhao, Z. Li, G.I.N. Waterhouse, R. Shi, J. Zhao, M. Zhang, L. Shang, G. Sheng, X. Zhang, X. Wen, L.-Z. Wu, C.-H. Tung, T. Zhang, Alumina-supported cofe alloy catalysts derived from layered-double-hydroxide nanosheets for efficient photothermal co2 hydrogenation to hydrocarbons, Adv. Mater. 30 (2018), 1704663, https://doi.org/10.1002/adma.201704663.

[58] Y. Liu, J. Zhao, J. Feng, Y. He, Y. Du, D. Li, Layered double hydroxide-derived Ni-Cu nanoalloy catalysts for semi-hydrogenation of alkynes: improvement of

selectivity and anti-coking ability via alloying of Ni and Cu, J. Catal. 359 (2018) 251–260, https://doi.org/10.1016/j.jcat.2018.01.009.
[59] X. Yu, M. Zhang, W. Yuan, G. Shi, A high-performance three-dimensional Ni–Fe layered double hydroxide/graphene electrode for water oxidation, J. Mater. Chem. A 3 (2015) 6921–6928, https://doi.org/10.1039/C5TA01034A.
[60] S.J. Kim, Y. Lee, D.K. Lee, J.W. Lee, J.K. Kang, Efficient co–fe layered double hydroxide photocatalysts for water oxidation under visible light, J. Mater. Chem. A 2 (2014) 4136, https://doi.org/10.1039/c3ta14933a.
[61] W.-J. Liu, L. Dang, Z. Xu, H.-Q. Yu, S. Jin, G.W. Huber, Electrochemical OXidation of 5-hydroxymethylfurfural with Nife Layered Double Hydroxide (Ldh) Nanosheet Catalysts, ACS Catal. 8 (2018) 5533–5541, https://doi.org/10.1021/acscatal.8b01017.
[62] F. Basile, G. Fornasari, M. Livi, F. Tinti, F. Trifirò, A. Vaccari, Performance of new Pt and Pt-Cu on hydrotalcite-derived materials for NOxstorage/reduction, Top. Catal. 30 (2004) 223–227, https://doi.org/10.1023/B:TOCA.0000029753.61106.ef.
[63] F.-A. He, L.-M. Zhang, Organo-modified ZnAl layered double hydroxide as new catalyst support for the ethylene polymerization, J. Colloid Interface Sci. 315 (2007) 439–444, https://doi.org/10.1016/j.jcis.2007.06.079.
[64] A. Rehor, N.E. Botterhuis, J.A. Hubbell, N. a J.M. Sommerdijk, N. Tirelli, Glucose sensitivity through oxidation responsiveness. an example of cascade-responsive nano-sensors, J. Mater. Chem. 15 (2005) 4006–4009, https://doi.org/10.1039/B510998A.
[65] D. Motta, F. Sanchez, K. Alshammari, L.E. Chinchilla, G.A. Botton, D. Morgan, T. Tabanelli, A. Villa, C. Hammond, N. Dimitratos, Preformed Au colloidal nanoparticles immobilised on NiO as highly efficient heterogeneous catalysts for reduction of 4-nitrophenol to 4-aminophenol, J. Environ. Chem. Eng. 7 (2019), 103381, https://doi.org/10.1016/j.jece.2019.103381.
[66] H. Deng, J. Yin, J. Ma, J. Zhou, L. Zhang, L. Gao, T. Jiao, Exploring the enhanced catalytic performance on nitro dyes via a novel template of flake-network Ni-Ti LDH/GO in-situ deposited with Ag3PO4 NPs, Appl. Surf. Sci. 543 (2021), 148821, https://doi.org/10.1016/j.apsusc.2020.148821.
[67] Z. Wei, Y. Li, L. Dou, M. Ahmad, H. Zhang, Cu3–xNixAl-layered double hydroxide-reduced graphene oxide nanosheet array for the reduction of 4-nitrophenol, ACS Appl. Nano Mater. 2 (2019) 2383–2396, https://doi.org/10.1021/acsanm.9b00273.
[68] E.T. Saw, U. Oemar, X.R. Tan, Y. Du, A. Borgna, K. Hidajat, S. Kawi, Bimetallic Ni–Cu catalyst supported on CeO2 for high-temperature water–gas shift reaction: methane suppression via enhanced CO adsorption, J. Catal. 314 (2014) 32–46, https://doi.org/10.1016/j.jcat.2014.03.015.
[69] C. Rudolf, B. Dragoi, A. Ungureanu, A. Chirieac, S. Royer, A. Nastro, E. Dumitriu, NiAl and CoAl materials derived from takovite-like LDHs and related structures as efficient chemoselective hydrogenation catalysts, Catal. Sci. Technol. 4 (2014) 179–189, https://doi.org/10.1039/C3CY00611E.
[70] J. Ashok, Y. Kathiraser, M.L. Ang, S. Kawi, Ni and/or Ni–Cu alloys supported over SiO 2 catalysts synthesized via phyllosilicate structures for steam reforming of biomass tar reaction, Catal. Sci. Technol. 5 (2015) 4398–4409, https://doi.org/10.1039/C5CY00650C.
[71] M.C. Biesinger, B.P. Payne, A.P. Grosvenor, L.W.M. Lau, A.R. Gerson, R.St. C. Smart, Resolving surface chemical states in XPS analysis of first row transition metals oxides and hydroxides: Cr Mn Fe Co and Ni, Appl. Surf. Sci. 257 (2011) 2717–2730, https://doi.org/10.1016/j.apsusc.2010.10.051.
[72] C. Mebrahtu, S. Perathoner, G. Giorgianni, S. Chen, G. Centi, F. Krebs, R. Palkovits, S. Abate, Deactivation mechanism of hydrotalcite-derived Ni–AlO x catalysts during low-temperature CO 2 methanation via Ni-hydroxide formation and the role of Fe in limiting this effect, Catal. Sci. Technol. 9 (2019) 4023–4035, https://doi.org/10.1039/C9CY00744J.
[73] H. Yoshida, H. Oyama, R. Shiomori, T. Hirakawa, J. Ohyama, M. Machida, Enhanced catalytic no reduction in no–co–c3h6–o2 reaction using pseudo-spinel (nicu)al2o4 supported on γ-Al2O3, ACS Catal. 11 (2021) 7302–7309, https://doi.org/10.1021/acscatal.1c01419.
[74] G. Giorgianni, C. Mebrahtu, M. Erwin Schuster, A. Ian Large, G. Held, P. Ferrer, F. Venturini, D. Grinter, R. Palkovits, S. Perathoner, G. Centi, S. Abate, R. Arrigo, Elucidating the mechanism of the CO 2 methanation reaction over Ni–Fe hydrotalcite-derived catalysts via surface-sensitive in situ XPS and NEXAFS, Phys. Chem. Chem. Phys. 22 (2020) 18788–18797, https://doi.org/10.1039/D0CP00622J.
[75] A.R. Naghash, T.H. Etsell, S. Xu, XRD and XPS Study of Cu−Ni interactions on reduced copper−nickel−aluminum oxide solid solution catalysts, Chem. Mater. 18 (2006) 2480–2488, https://doi.org/10.1021/cm051910o.
[76] A. Aldureid, F. Medina, G.S. Patience, D. Montané, Ni-Cu/Al2O3 from layered double hydroxides hydrogenates furfural to alcohols, Catalysts 12 (2022) 390, https://doi.org/10.3390/catal12040390.
[77] M. Gazzano, W. Kagunya, D. Matteuzzi, A. Vaccari, Neutron diffraction studies of polycrystalline ni/mg/al mixed oxides obtained from hydrotalcite-like precursors, J. Phys. Chem. B 101 (1997) 4514–4519, https://doi.org/10.1021/jp963761q.
[78] F. Basile, G. Fornasari, M. Gazzano, A. Vaccari, Rh, Ru and Ir catalysts obtained by HT precursors: effect of the thermal evolution and composition on the material structure and use, J. Mater. Chem. 12 (2002) 3296–3303, https://doi.org/10.1039/B205146J.
[79] C. Wang, W. Zou, J. Wang, Y. Ge, R. Lu, S. Zhang, Insight into the mechanism of gold-catalyzed reduction of nitroarenes based on the substituent effect and in situ IR, New J. Chem. 41 (2017) 3865–3871, https://doi.org/10.1039/C7NJ00157F.
[80] T. Raventos-Duran, M. Camredon, R. Valorso, C. Mouchel-Vallon, B. Aumont, Structure-activity relationships to estimate the effective Henry's law constants of organics of atmospheric interest, Atmos. Chem. Phys. 10 (2010) 7643–7654, https://doi.org/10.5194/acp-10-7643-2010.
[81] D. Andreou, D. Iordanidou, I. Tamiolakis, G. Armatas, I. Lykakis, Reduction of nitroarenes into aryl amines and n-aryl hydroxylamines via activation of nabh4 and ammonia-borane complexes by ag/tio2 catalyst, Nanomaterials 6 (2016) 54, https://doi.org/10.3390/nano6030054.
[82] Y. Huang, K. Zheng, X. Liu, X. Meng, D. Astruc, Optimization of Cu catalysts for nitrophenol reduction click reaction and alkyne coupling, Inorg. Chem. Front. 7 (2020) 939–945, https://doi.org/10.1039/C9QI01449G.
[83] L. Jin, G. He, J. Xue, T. Xu, H. Chen, Cu/graphene with high catalytic activity prepared by glucose blowing for reduction of p-nitrophenol, J. Clean. Prod. 161 (2017) 655–662, https://doi.org/10.1016/j.jclepro.2017.05.162.
[84] K.Ch Das, S.S. Dhar, Fast catalytic reduction of p-nitrophenol by Cu/HAP/ZnFe2O4 nanocomposite, Mater. Sci. Eng.: B 263 (2021), 114841, https://doi.org/10.1016/j.mseb.2020.114841.